iScience

Article

Postnatal hyperosmolality alters development of hypothalamic feeding circuits with context-specific changes in ingestive behavior

Highlights

- PVH neurons receive convergent signals conveying fluid and energy status
- Postnatal hyperosmotic stimulation increases innervation of PVH by AgRP neurons
- Early osmotic stimulation causes context-specific changes in ingestive behavior

Authors

Serena R. Sweet, Jessica E. Biddinger, Jessie B. Zimmermann, Gina L. Yu, Richard B. Simerly

Correspondence

richard.simerly@vanderbilt.edu

In brief

Developmental biology; Developmental neuroscience; Neuroscience

Sweet et al., 2025, iScience *28*, 112284
May 16, 2025
https://doi.org/10.1016/j.isci.2025.112284

CellPress

iScience

CellPress
OPEN ACCESS

Article

Postnatal hyperosmolality alters development of hypothalamic feeding circuits with context-specific changes in ingestive behavior

Serena R. Sweet,[1,2,3,4] Jessica E. Biddinger,[1,2,3] Jessie B. Zimmermann,[1] Gina L. Yu,[1] and Richard B. Simerly[1,2,3,5,*]
[1]Department of Molecular Physiology & Biophysics, Vanderbilt University, Nashville, TN 37232, USA
[2]Vanderbilt Center for Addiction Research, Vanderbilt University, Nashville, TN 37232, USA
[3]Vanderbilt Brain Institute, Vanderbilt University, Nashville, TN 37232, USA
[4]Senior author
[5]Lead contact
*Correspondence: richard.simerly@vanderbilt.edu
https://doi.org/10.1016/j.isci.2025.112284

SUMMARY

Drinking and feeding are tightly coordinated homeostatic events and the paraventricular nucleus of the hypothalamus (PVH) represents a possible node of neural integration for signals related to energy and fluid homeostasis. We used *TRAP2;Ai14* mice and Fos labeling to visualize neurons in the PVH and median preoptic nucleus (MEPO) responding to both water deprivation and feeding signals. We determined that structural and functional development of dehydration-sensitive inputs to the PVH precedes those of agouti-related peptide (AgRP) neurons, which convey hunger signals and are known to be developmentally programmed by nutrition. Moreover, we found that osmotic hyperstimulation of neonatal mice led to enhanced AgRP inputs to the PVH in adulthood, as well as disruptions to ingestive behaviors during high-fat diet feeding and dehydration-anorexia. Thus, development of feeding circuits is impacted not only by nutritional signals, but also by early perturbations to fluid homeostasis with context-specific consequences for coordination of ingestive behavior.

INTRODUCTION

An essential role of the hypothalamus is to coordinate multiple physiological functions and ensure homeostasis in the face of dynamic environmental changes and behavioral requirements. Eating and drinking represent tightly coordinated activities controlled by the hypothalamus.[1–6] Water restriction leads to a robust reduction in food intake, a phenomenon called dehydration-anorexia, which is rapidly reversed when water is presented.[7–10] In addition to dehydration-anorexia, prandial thirst illustrates the close coordination between feeding and drinking; during food intake drinking is initiated to regulate fluids lost during meal consumption.[11–13] Such coordination requires effective integration of sensory signals conveyed to the hypothalamus by neurons that respond directly to a variety of physiological signals related to metabolic state or fluid homeostasis.[14–16]

How this integration is accomplished is not fully known but likely involves convergence of neuroendocrine sensory pathways onto common hypothalamic targets. The paraventricular nucleus of the hypothalamus (PVH) represents such a target region and plays a central role in regulating both fluid and energy balance.[1,3,6,17,18] The PVH receives direct inputs from neurons containing orexigenic agouti related peptide (AgRP) in the arcuate nucleus of the hypothalamus (ARH) that convey negative valence signals associated with hunger.[19–24] PVH neurons also receive signals related to thirst or osmotic dehydration from the median preoptic nucleus (MEPO) located in the lamina terminalis.[14,25,26] Information about hyperosmotic state is conveyed through the blood via activation of neurons in the organum vasculosum of the lamina terminalis (OVLT) and subfornical organ (SFO), and this information is relayed to the MEPO to drive water intake.[27–32] Accordingly, Fos labeling is elevated in the PVH of osmotically dehydrated animals and in response to optogenetic activation of MEPO neurons.[31,33,34] Hunger signals resulting from fasting, or injections of 2-deoxyglucose that mimic energy deficit, also induce Fos labeling in similar components of the PVH.[35,36] Moreover, calcium imaging studies identified molecularly defined ensembles of PVH neurons that respond to both drinking and food intake.[6] Together, these observations suggest that the PVH is a likely site for convergence of signals related to thirst and hunger.[30,37,38]

Although projections from the ARH are formed during the first two weeks of postnatal life, a time of considerable developmental plasticity, the development of convergent hypothalamic pathways is largely unknown.[19,39–42] Neurons expressing agouti-related peptide (AgRP) and proopiomelanocortin (POMC) are born prenatally but extend their axons from the ARH to innervate the PVH primarily during the second week of life, and postnatal perturbations in metabolic stimuli, such as leptin secretion, disturb targeting of AgRP axons in the PVH.[43–53] Moreover, manipulating the activity of AgRP neurons impairs the neurotrophic action of leptin on AgRP projections to the

PVH, and offspring of dams fed a high-fat diet just during lactation have impaired innervation of the PVH by AgRP and are predisposed to obesity in adulthood.[54–56] Such environmental effects on development of feeding circuitry are considered developmental programming, but how hypothalamic circuits conveying thirst signals develop has received little attention.[40,41,57–60] Neonatal mice rely on milk from dams for both nutrition and hydration, but it remains unclear if they are motivated by thirst, hunger, or stimuli associated with maternal attachment.[61–64] Injections of hypertonic saline induce Fos labeling in the SFO, OVLT, and PVH of 2-day-old rats, indicating that pathways for osmotic dehydration signals are intact at an early age.[34] In contrast, leptin injections do not activate PVH neurons until after they have received significant innervation from the ARH and begin transitioning to consumption of solid food.[19,62,65]

To identify neurons that receive convergent thirst and hunger signals in the PVH, we used adult TRAP2/Ai14 mice to permanently label PVH neurons that respond to thirst combined with Fos labeling to visualize neurons that respond to fasting.[66] In addition, we mapped the ontogeny of neuronal activation in the MEPO and PVH resulting from acute hypernatremia to visualize cells responding to osmotic dehydration. We determined that projections from the MEPO to the PVH precede those arriving from the ARH and that daily exposure to hyperosmotic stimuli during early postnatal life leads to enhanced innervation of the MEPO and PVH by AgRP neurons in adult male mice, which is associated with context-specific changes to drinking and feeding.

RESULTS

Drinking and feeding signals converge in the MEPO and PVH of adult mice

Water deprivation induces Fos labeling in substantial populations of neurons located in both the MEPO and PVH, and food deprivation induces robust Fos expression in the ARH and PVH.[8,33] To simultaneously visualize neurons activated by both feeding and drinking, we used the FosTRAP transgenic mouse line, *TRAP2*, in which *2A-iCreER^{T2}* was knocked into the *Fos* locus. In *TRAP2;Ai14* double transgenic mice, neuronal activation results in the expression of CreER, which enters the nucleus in response to a 4-hydroxytamoxifen (4-OHT) and induces Cre-mediated recombination, leading to permanent expression of tdTomato in active neurons.[66] Injecting 4-OHT into *TRAP2;Ai14* double transgenic mice resulted in a marked induction of tdTomato+ labeling in the MEPO (Figures 1A–1C) and PVH (Figures 1D–1G) of mice deprived of water for 36h (Thirst-TRAP) compared to euhydrated controls (EUH-TRAP). Thirst-TRAPped cells in the PVH were not domain specific, with the magnocellular and parvocellular cells of the PVH exhibiting a significantly higher induction in Thirst-TRAP mice compared to EUH-TRAP controls. Immunohistochemical analysis of labeled neurons revealed that the Thirst-TRAPped cells in the PVH represent a mixed population of neurons that include vasopressin (Figures S1A-S1C), oxytocin (Figures S1D–S1F), and nNOS (Figures S1G–S1I) neurons, which are all thought to be involved in regulation of fluid homeostasis.[27,31,67] In contrast, there were no differences in tdTomato+ labeling in the ARH in Thirst-TRAP mice compared to EUH-TRAP controls (S2A-S2C). After Thirst-TRAP, we challenged all mice with a 23h fast followed by *ad-libitum* refeeding 1h before perfusion and tissue collection (Hunger-Fos) to capture the maximal number of activated neurons involved in the transition between fasting and refeeding. There were no differences in neurons displaying enhanced Fos-labeling following a fast-refeed challenge (Hunger-Fos+) in the MEPO (Figures 1H–1J), PVH (Figures 1K–1N), and ARH (Figures S2D–S2F) of EUH-TRAP and Thirst-TRAP groups following fast-refeeding. Significantly more Hunger-Fos+ cells co-labeled as Thirst-TRAPped cells were observed in the MEPO compared to EUH-TRAP controls (Figures 1O–1Q). Similarly, greater numbers of doubly labeled cells were identified in both the magnocellular and parvocellular compartments of the PVH (Figures 1R–1U). We did not detect doubly labeled neurons in ARH (Figures S2G–S2I). These results suggest that dehydration signals in adult mice activate sub-populations of neurons in the MEPO and PVH, whereas signals related to the transition from the fasting to fed state activate sub-populations of neurons in the MEPO, PVH, and ARH, and that convergence of these signals is detected in both the MEPO and PVH.

MEPO neurons project to the PVH during the first week of life

Although direct projections from the MEPO to the PVH are known to be important for fluid homeostasis in adults, whether these projections are in place in neonatal mice has yet to be established. To visualize the MEPO projections to the PVH in neonatal mice, we used DiI axonal labeling in wild-type neonatal mice perfused at postnatal day (P)8 (Figure 2A). Single DiI crystals were implanted in the MEPO (Figures 2B–2D) using an insect needle and brains were incubated in fixative for 6 weeks. We observed a moderate density of labeled axons extending caudally from the MEPO and remaining largely confined to the periventricular zone of the hypothalamus. Moreover, MEPO neurons appear to provide at least a moderate density of DiI labeled axons in the PVH (Figures 2E–2G). These results suggest that neural projections from the MEPO to the PVH are intact in early postnatal life.

Ontogeny of MEPO and PVH neurons responding to osmotic stimuli

The DiI labeling results establish that neurons in the MEPO project to the PVH early in postnatal life, but whether these neurons are capable of responding to dehydration signals and conveying this information to the PVH early in postnatal life in mice is unknown. Therefore, we investigated development of the functional capacity of projections from the MEPO to the PVH by visualizing Fos immunolabeling in response to a dehydration stimulus. Subcutaneous (s.c.) administration of 0.1 mL/10g BW of 2.0M NaCl (hypertonic saline, HS), or of 0.9% NaCl (isotonic saline, IS), were given to male mice at P1, P8, P16, and P30. Significant increases in Fos labeling were observed in the MEPO at P1, P8, P16, and P30 in HS-treated mice compared to IS-treated controls (Figures 3A–3L), indicating that MEPO neurons are capable of responding to osmotic signals at birth. Moreover, significantly more HS-induced Fos-immunoreactive nuclei were detected in the PVH at P1, compared to controls, suggesting that

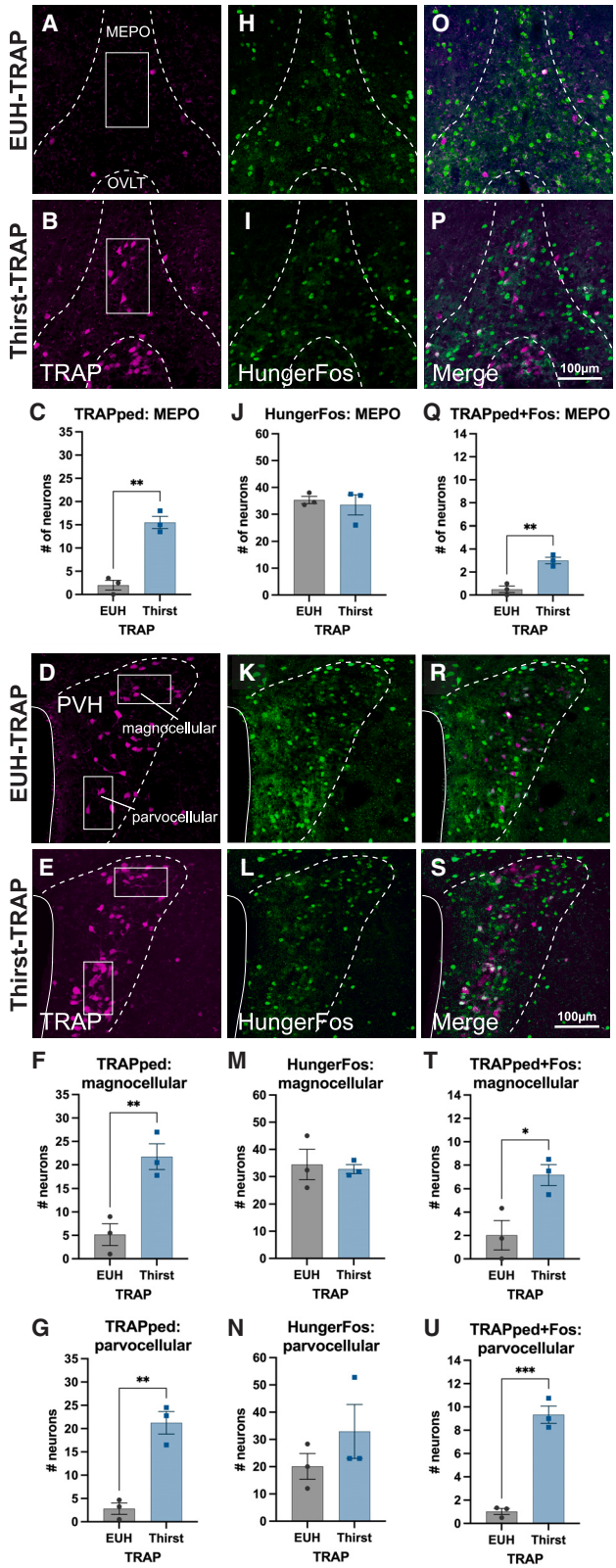

Figure 1. Drinking and feeding signals converge in the MEPO and PVH of adult mice

(A and B) Representative confocal images showing TRAPped (tdTomato+) cells in the MEPO of both EUH-TRAP (A) and Thirst-TRAP (B) mice. A region of interest (ROI) is indicated by the white rectangle.

(C) Quantification of number of cells expressing tdTomato+ in the MEPO ROI.

(D and E) Representative confocal images showing TRAPped (tdTomato+) cells in the PVH of both EUH-TRAP (D) and Thirst-TRAP (E) mice. ROIs within the magnocellular and parvocellular compartments are indicated by the white rectangles.

(F) Quantification of cells expressing tdTomato+ in the magnocellular ROI of the PVH.

(G) Quantification of cells expressing tdTomato+ in the parvocellular ROI of the PVH.

(H and I) Representative confocal images showing Fos+ cells in the MEPO in response to a fast-refeed stimulus (Hunger-Fos) in both EUH-TRAP (H) and Thirst-TRAP (I) mice.

(J) Quantification of immunohistochemical (IHC) analysis of cells expressing Fos+ in the MEPO ROI.

(K and L) Representative confocal images showing Fos+ cells in the PVH in response to a fast-refeed stimulus (Hunger-Fos) in both EUH-TRAP (K) and Thirst-TRAP (L) mice.

(M) Quantification of IHC analysis of cells expressing Fos+ in the magnocellular ROI of the PVH.

(N) Quantification of IHC analysis of cells expressing Fos+ in the parvocellular ROI of the PVH.

(O and P) Representative confocal images showing co-labeled tdTomato+/Fos+ cells in the MEPO in both EUH-TRAP (O) and Thirst-TRAP (P) mice.

(Q) Quantification of IHC analysis of co-labeled tdTomato+/Fos+ cells in the MEPO ROI.

(R and S) Representative confocal images showing co-labeled tdTomato+/Fos+ cells in the PVH in both EUH-TRAP (R) and Thirst-TRAP (S) mice.

(T) Quantification of IHC analysis co-labeled tdTomato+/Fos+ cells in the magnocellular compartment of the PVH.

(U) Quantification of IHC analysis of co-labeled tdTomato+/Fos+ cells in the parvocellular compartment of the PVH. All data are represented as mean ± SEM and data points are quantified across 1-2 sections for individual animals. Thirst-TRAP ($n = 3$), and EUH-TRAP ($n = 3$), where n represents the number of mice; Unpaired t-test: $^{*}p < 0.05$, $^{**}p < 0.01$, $^{***}p < 0.001$. Scale bars, 100μm. See also Figures S1 and S2.

dehydration signals are conveyed from the MEPO to the PVH as early as the first postnatal day (Figures 3M, 3Q, and 3U). Consistent with the timeline for development of inputs from MEPO to PVH, we observed a significant induction of Fos in the PVH at P8 (Figures 3N, 3R, and 3V), as well as at P16 and P30 compared to controls (Figures 3O, 3P, 3S, 3T, 3W, and 3X). Notably, the maximum density of Fos labeling in the MEPO was observed by P8 (Figure 3Y). The ontogeny of Fos induction in the PVH following osmotic signals contrasted with the later achievement of maximal levels of Fos labeling in the PVH at P16 (Figure 3Z), which coincides with early maturation of projections from AgRP neurons. Together, these results suggest MEPO and PVH neurons are responding to osmotic signals as early as P1, with a graded maximal response coinciding with the early divergence of feeding and drinking behavior.

Postnatal perturbation of fluid homeostasis impacts development of projections from AgRP and POMC neurons to the MEPO and PVH

To determine if activation of neurons during osmotic dehydration alters innervation of the PVH by AgRP and POMC neurons, we

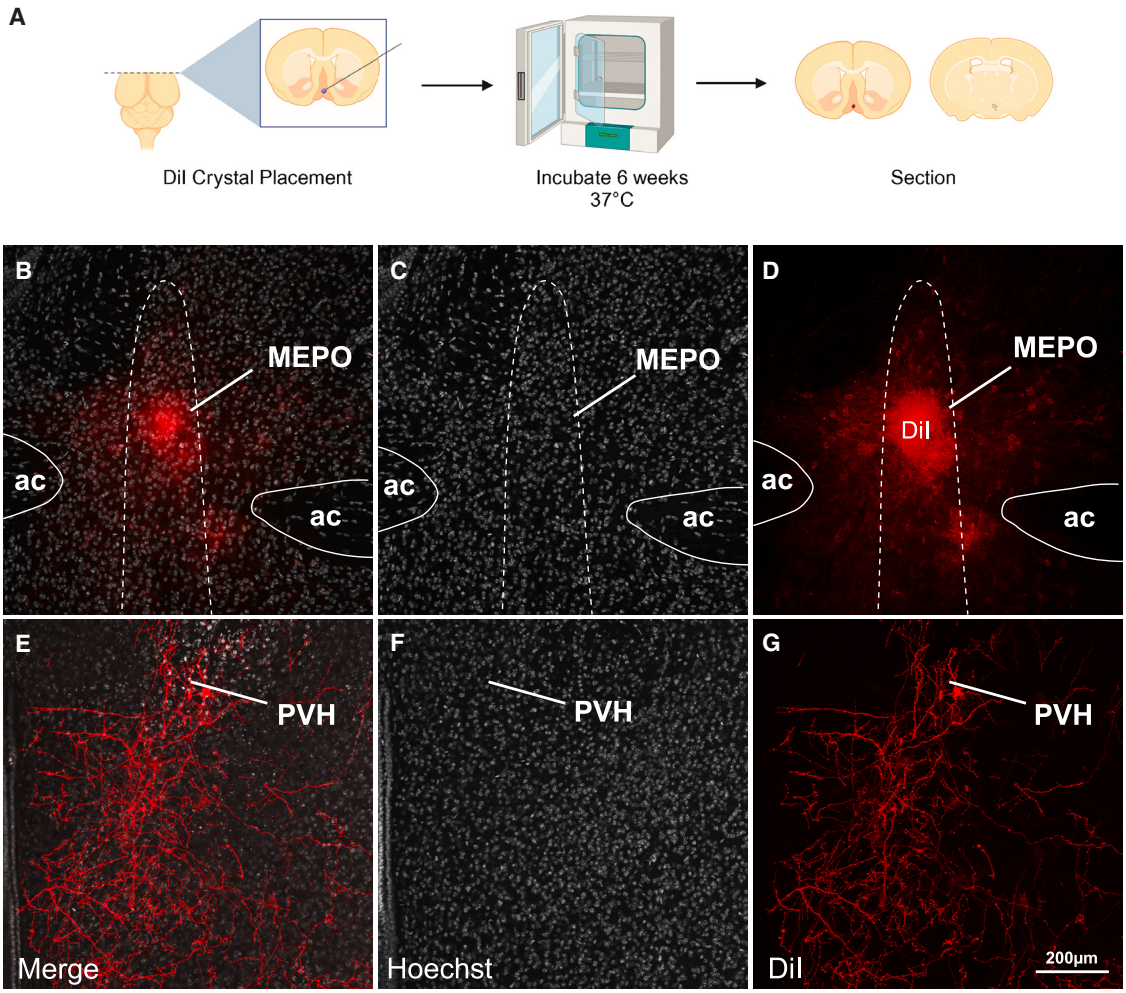

Figure 2. Postnatal developmental projections from the MEPO to the PVH

(A) Schematic of experiment design, showing brains from P8 male mice were sectioned from rostral to caudal so as to expose the MEPO and single DiI crystals were implanted in the MEPO using an insect needle, the brains were then placed back into fixative and incubated for 5–6 weeks, and then sectioned on a vibratome.

(B–D) Confocal images showing Hoechst Dye and implant location of DiI crystal in the MEPO.

(E–G) Confocal images showing Hoechst Dye and downstream robust DiI axonal labeling in the PVH. Images are collected from one animal. Scale bars, 200μm.

adapted an HS-injection protocol used previously in adult mice to model developmental disruption of fluid homeostasis by administering postnatal (PN) daily injections of hypertonic saline (HS^{PN}) or isotonic saline (IS^{PN}) from P5-P15, and then assessed densities of projections from AgRP and β-endorphin neurons to the MEPO and PVH in adulthood.[29] Compared to IS^{PN} control mice, the density of AgRP axons in HS^{PN} mice is significantly elevated in the MEPO (Figures 4A–4C) and in the PVH (Figures 4E–4G). HS^{PN} mice also showed a significant decrease in the density of β-endorphin axons in the MEPO (Figures 4I–4K), but not in the PVH (Figures 4M–4O). As a control, we used a separate cohort of postweaning (PW) mice and administered daily injections of hypertonic saline (HS^{PW}) or isotonic saline (IS^{PW}) from P28 to P38 to determine if the action of the HS treatments is limited to the early postnatal period when AgRP neurons are extending axons to downstream targets. In contrast to our observations in adult HS^{PN} mice, adult HS^{PW} mice exhibited no change in densities of AgRP or β-endorphin axons and terminals in the MEPO (Figures 4D, 4L and S3A–S3D) or PVH (Figures 4H, 4P and S3E–S3H), consistent with there being a critical period for developmental programming of AgRP and β-endorphin projections.[47,50] Notably, treatment of adult HS^{PN} mice with acute injections of HS (150ul of 2.0M NaCl) before tissue collection did not result in altered levels of Fos induction in the MEPO (Figures S3I–S3K) or PVH (Figures S3L–S3N) compared to that observed in IS^{PN} mice, which suggests that the postnatal HS treatments do not have a sustained adverse effect on osmotic signaling from the MEPO to the PVH. Together, these results suggest that development of neurons involved in feeding are impacted by the stimulation of neural circuits involved in drinking during postnatal life, without deleterious effects on the function of drinking circuitry in adulthood.

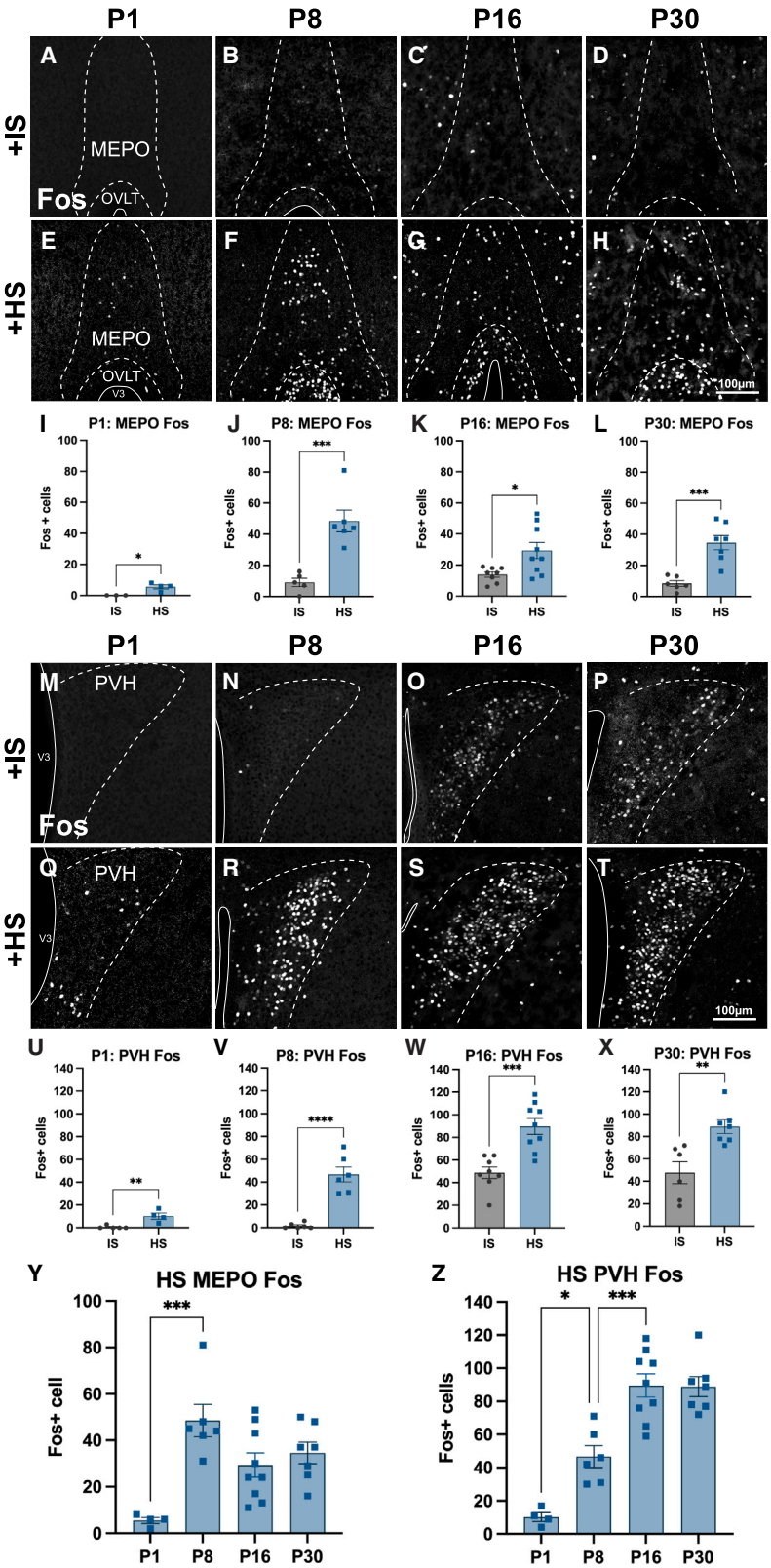

Figure 3. Ontogeny of circuits responding to osmotic stimuli

(A–D) Representative confocal images showing Fos+ cells in the MEPO of neonatal mice across ages P1 (A), P8 (B), P16 (C), and P30 (D) treated with a subcutaneous (s.c.) administration of 0.1mL/10g BW of 0.9% NaCl (isotonic saline, IS) as a control.

(E–H) Representative confocal images showing Fos+ cells in the MEPO of neonatal mice at ages P1 (E), P8 (F), P16 (G), and P30 (H) treated with s.c. administration of 0.1mL/10g BW of 2.0M NaCl as a dehydration stimulus (hypertonic saline, HS).

(I) Quantification of IHC analysis of Fos+ cells in the MEPO at P1. IS (n = 3), and HS (n = 4).

(J) Quantification of IHC analysis of Fos+ cells in the MEPO at P8. IS (n = 5), and HS (n = 6).

(K) Quantification of IHC analysis of Fos+ cells in the MEPO at P16.IS (n = 8), and HS (n = 9).

(L) Quantification of IHC analysis of Fos+ cells in the MEPO at P30. IS (n = 6), and HS (n = 7).

(M–P) Representative confocal images showing Fos+ cells in the PVH of neonatal mice across ages P1 (M), P8 (N), P16 (O), and P30 (P) treated with an s.c. administration of 0.1mL/10g BW of 0.9% NaCl as a control (IS).

(Q–T) Representative confocal images showing Fos+ cells in the PVH of neonatal mice at ages P1 (Q), P8 (R), P16 (S), and P30 (T) treated with s.c. administration of 0.1mL/10g BW of 2.0M NaCl as a dehydration stimulus (HS).

(U) Quantification of IHC analysis of Fos+ cells in the PVH at P1. IS (n = 5) and HS (n = 4).

(V) Quantification of IHC analysis of Fos+ cells in the PVH at P8. IS (n = 6) and HS (n = 6).

(W) Quantification of IHC analysis of Fos+ cells in the PVH at P16. IS (n = 8) and HS (n = 9).

(X) Quantification of IHC analysis of Fos+ cells in the PVH at P30. IS (n = 6) and HS (n = 7).

(Y) Comparison of Fos+ cells in the MEPO of HS mice across ages. One-way ANOVA with multiple comparisons.

(Z) Comparison of Fos+ cells in the MEPO of HS mice across ages. One-way ANOVA with multiple comparisons.

All data are represented as mean ± SEM and data points are quantified across 1 section for individual animals; n represents the number of animals; Unpaired t-test: *p < 0.05, **p < 0.01, ***p < 0.001. Scale bars, 100μm.

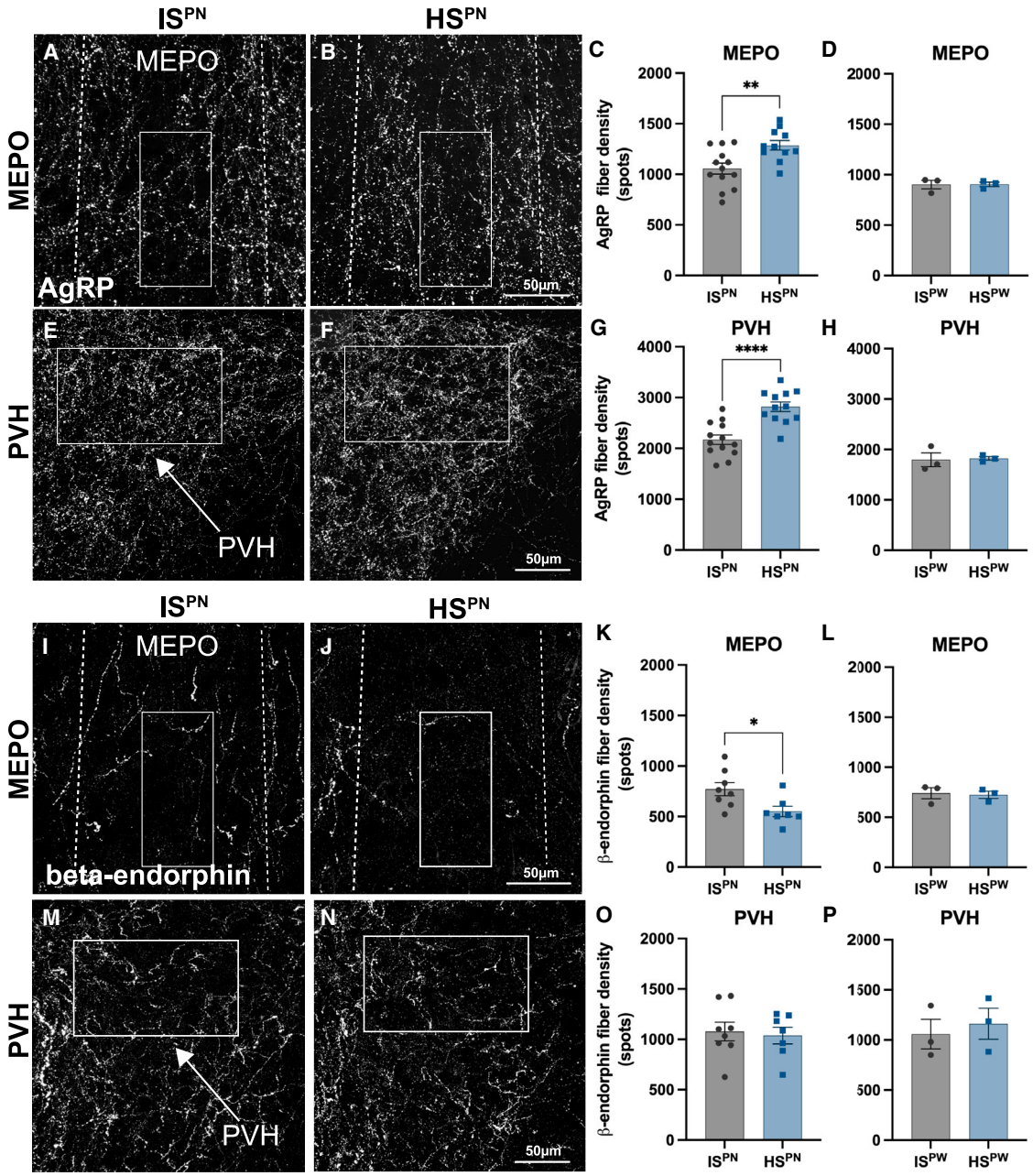

Figure 4. Postnatal perturbation to fluid homeostasis impacts development of AgRP projections to the MEPO and PVH

(A and B) Representative confocal images showing AgRP fiber densities in the MEPO of adult mice treated daily from P5-P15 with either s.c administration of 0.9% NaCl as a control (IS^{PN}; A) or 2.0M NaCl as a dehydration stimulus (HS^{PN}, B). Regions of interest (ROIs) are indicated by the white rectangles.

(C) Quantification of IHC analysis of AgRP fiber densities in the MEPO ROI of IS^{PN} and HS^{PN} mice using the spots feature in Imaris software. IS^{PN} ($n = 13$) and HS^{PN} ($n = 11$).

(D) Quantification of IHC analysis of AgRP fiber densities in the MEPO ROI of IS^{PW} and HS^{PW} mice using the spots feature in Imaris software. IS^{PW} ($n = 3$) and HS^{PW} ($n = 3$).

(E and F) Representative confocal images showing AgRP fiber densities in the PVH of IS^{PN} (E) and HS^{PN} (F) mice.

(G) Quantification of IHC analysis of AgRP fiber densities in the PVH ROI using the spots feature in Imaris software. IS^{PN} ($n = 13$), and HS^{PN} ($n = 12$).

(H) Quantification of IHC analysis of AgRP fiber densities in the PVH ROI of IS^{PW} and HS^{PW} mice using the spots feature in Imaris software. IS^{PW} ($n = 3$) and HS^{PW} ($n = 3$).

(I and J) Representative confocal images showing β-endorphin fiber densities in the MEPO of adult IS^{PN} (I) and HS^{PN} (J) mice. Regions of interest (ROIs) are indicated by the white rectangles.

(K) Quantification of IHC analysis of β-endorphin fiber densities in the MEPO ROI using the spots feature in Imaris software. IS^{PN} ($n = 8$), and HS^{PN} ($n = 7$).

(legend continued on next page)

Hyperstimulation of drinking circuits during postnatal development leads to increases in water intake during HFD feeding in adults

Because osmotic dehydration altered the density of AgRP inputs to the PVH, we examined ingestive behavior in mice exposed to HS during the postnatal period. A cohort of adult HS^{PN} and IS^{PN} mice were singly housed in metabolic profiling chambers with *ad libitum* access to standard chow (normal chow diet, NCD) and water for 5 days, followed by data collection for 7 days with access to high-fat diet (HFD). When fed NCD, HS^{PN} mice did not display a difference in body weight (Figure S4A), water intake (Figure S4B), or food intake (Figure S4C) compared to IS^{PN} controls. Moreover, HS^{PN} mice did not display a significant change in HFD food intake compared to IS^{PN} controls (Figures 5A and 5B), but HS^{PN} mice displayed a significant increase in cumulative water intake during HFD exposure (Figures 5C and 5D). Another cohort of adult HS^{PN} and IS^{PN} mice were singly housed and given *ad libitum* access to an HFD for 20 weeks to assess long-term effects on body weight. Although all mice displayed increased body weight when exposed to a long-term HFD, no differences in body weight were observed between groups (Figure S4D). These data suggest that early perturbations to fluid homeostasis have a lasting effect on ingestive behavior that appears to be diet- and context-dependent.

Hyperstimulation of drinking circuits during postnatal development leads to a sustained dehydration-anorexic response and sustained decrease in water intake after a fast-refeed challenge in adults

Because feeding and drinking are linked behaviors, we adapted a model of dehydration-anorexia (DE-anorexia) to determine if HS^{PN} mice show normal anorexic responses to dehydration in adulthood.[7,9,10,36] A cohort of adult HS^{PN} and IS^{PN} mice were singly housed in metabolic profiling chambers with *ad libitum* access to food and water for a 4-day acclimation period, followed by a 48h dehydration period (DEH), and a subsequent 4-day period of rehydration (REH). HS^{PN} mice did not display a difference in water intake for the entire duration of the experiment (Figures S5A–S5D). Although HS^{PN} mice did not display a significant change in food intake 48h before dehydration or during the 48h dehydration period (Figures 6A–6D), there was a significant and sustained decrease in food intake during the first 48h of the rehydration period (Figures 6A, 6B, and 6E). A different cohort of adult HS^{PN} and IS^{PN} mice were singly housed in metabolic chambers and exposed to a fast-refeed challenge where food was removed from the cage for 24h and then replaced. There were no changes to food intake (Figures S5E and S5F) or water intake during the inactive light period, before, during, or after the fast (Figure 6F), however, HS^{PN} mice displayed a significant decrease in water intake during the active dark period after refeeding (Figure 6G). Together, these results suggest that osmotic dehydration during postnatal development permanently perturbs patterns of ingestion with deprivation-specific changes, revealing perturbations to fluid homeostasis as a novel effector of developmental programming.

DISCUSSION

Neural connections between hypothalamic nuclei develop primarily during postnatal life and appear to be sensitive to alterations in a variety of environmental factors during this period.[43–49] Our results indicate that projections from MEPO neurons to the PVH are established early in postnatal life and precede mature patterning of AgRP inputs to the PVH from the ARH. As early as the first day of life (P1) signals conveying osmotic stimuli activate neurons in the MEPO and PVH. Peak levels of Fos labeling in the PVH appear to be delayed, suggesting that HS-induced neuronal activation in the PVH requires complete innervation by the MEPO to fully respond to such an osmotic stimulus. We also observed enhanced densities of AgRP terminals in the PVH of mice that received hyperstimulation of thirst circuits by postnatal osmotic dehydration. This observation suggests that afferents to the PVH from osmotically activated MEPO neurons may influence development of convergent AgRP afferents, and that such circuitry defects could correspond to observed context-specific changes in ingestive behavior. Together, these results suggest a new model of developmental programming that links postnatal exposure to hyperosmotic dehydration stimuli and development of feeding circuits.

Our thirst and hunger double-labeling results in adult TRAP2 mice demonstrate that a subpopulation of neurons located in a restricted domain of the PVH represents a cellular mode of action for convergence of signals conveying thirst signals with those related to feeding. Although this is the first clear demonstration that individual neurons respond to both thirst and feeding signals, previous evidence from both rat and mouse models identified the PVH as a likely node of sensory integration for coordination of drinking and food intake.[36] Previous work established that osmotic dehydration signals are sensed by the SFO and OVLT and then conveyed to the MEPO and PVH, however, ablation of MEPO or PVH, but not the circumventricular organs, abolishes dehydration-induced drinking.[17,31] Signals from AgRP neurons convey hunger signals to the PVH that are involved in regulation of feeding, but the presence of Fos labeling in the MEPO in fast-refeed mice in our study suggests that a subpopulation of these neurons may also respond to both thirst and hunger and likely represent an additional level of convergence for signals that coordinate drinking and feeding.[18,22,68,69]

The number of neurons in the PVH we detected that are doubly labeled likely represent a conservative estimate for numbers of

(L) Quantification of IHC analysis of β-endorphin fiber densities in the MEPO ROI of IS^{PW} and HS^{PW} mice using the spots feature in Imaris software. IS^{PW} ($n = 3$) and HS^{PW} ($n = 3$).
(M and N) Representative confocal images showing β-endorphin fiber densities in the PVH of IS^{PN} (M) and HS^{PN} (N) mice.
(O) Quantification of IHC analysis of β-endorphin fiber densities in the PVH ROI using the spots feature in Imaris. IS^{PN} ($n = 8$), and HS^{PN} ($n = 7$).
(P) Quantification of IHC analysis of β-endorphin fiber densities in the PVH ROI of IS^{PW} and HS^{PW} mice using the spots feature in Imaris software. IS^{PW} ($n = 3$) and HS^{PW} ($n = 3$). All data are represented as mean ± SEM and data points are quantified across 1 section for individual animals; n represents the number of animals; Unpaired t-test: $^{*}p < 0.05$, $^{**}p < 0.01$, $^{***}p < 0.001$. Scale bars, 50μm. See also Figure S3.

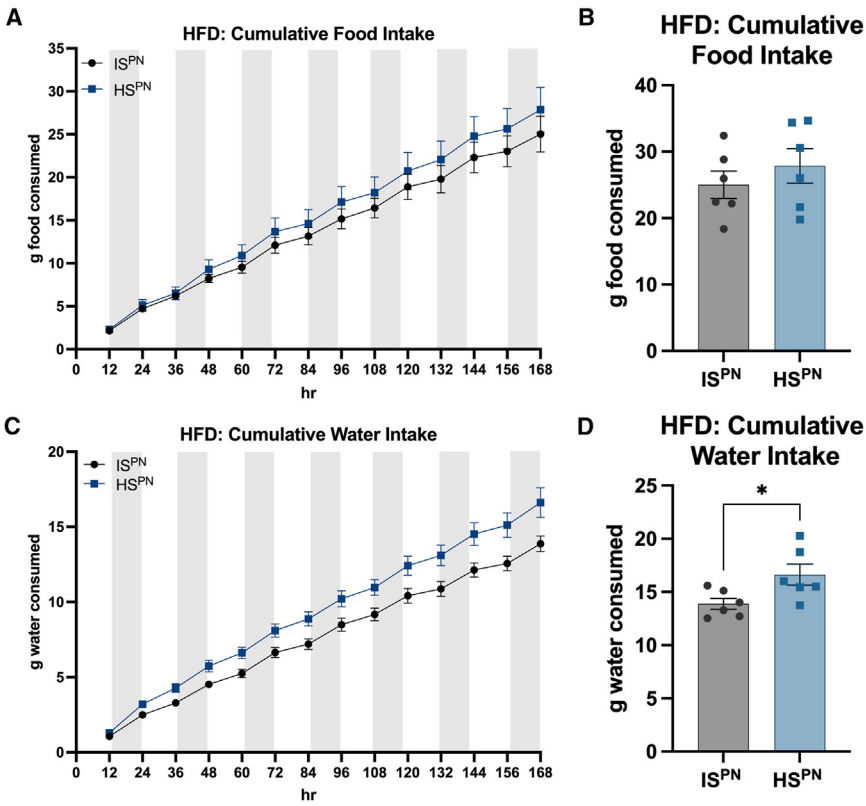

Figure 5. Hyperstimulation of drinking circuits during postnatal development increases water intake in the context of an HFD

(A) Quantification of cumulative food intake during the 168h (7 days) of HFD exposure in IS^{PN} ($n = 6$) and HS^{PN} ($n = 6$) animals. two-way ANOVA: no significant effect of treatment over time ($p = 0.7423$). Data are presented as group mean values ±SEM.

(B) Comparison of final cumulative food intake during HFD exposure. IS^{PN} ($n = 6$) and HS^{PN} ($n = 6$).

(C) Quantification of cumulative water intake during the HFD exposure. IS^{PN} ($n = 6$) and HS^{PN} ($n = 6$). two-way ANOVA: a significant main effect of treatment and time ($p < 0.0001$). Data are presented as group mean values ±SEM.

(D) Comparison of final cumulative water intake during HFD exposure. IS^{PN} ($n = 6$) and HS^{PN} ($n = 6$). Data in (B, D) are represented as mean ± SEM and data points are individual animals; n represents the number of animals; Unpaired t-test: $^{*}p < 0.05$, $^{**}p < 0.01$, $^{***}p < 0.001$. See also Figure S4.

neurons capable of responding to convergent sensory stimuli. Whether this low number of overlapping neurons is due to technical limitations or biological constraints is unclear, but because Fos labeling identifies only those neurons with detectable Fos expression at the time of perfusion, it is unlikely that the density of labeling detected represents maximum numbers of neurons activated by the fast-refeed challenge. Furthermore, the tdTomato+ labeling resulting from activity-dependent expression of Cre-recombinase identifies neurons receiving the cumulative effects of dehydration only during the 6h of 4-OHT action, which could also result in a conservative estimate of labeled neurons. Nevertheless, the density of double-labeled tdTomato+/Fos+ cells in the MEPO and PVH responding to sequential dehydration and fasting indicate that feeding and drinking signals are linked at a cellular level in a distinct subpopulation of PVH neurons.

Moreover, tdTomato+ neurons responding to a dehydration stimulus (Thirst-TRAP) appear to have regionally specific overlap with cell types involved in fluid homeostasis. A large portion of Thirst-TRAPped cells in the PVH express vasopressin, which are known to be key mediators of fluid homeostasis. Thirst-TRAPped neurons in the PVH were also identified as oxytocin neurons, consistent with suggestions that these cells are involved in renal control of fluid homeostasis. In addition, we identified a small population of Thirst-TRAPped neurons that express nNOS, which have been suggested to participate in circuits that affect ingestive behavior.[27,31,67,70–72] Although we were able to determine the identity of three subpopulations of PVH neurons that respond to dehydration, it is likely that a comprehensive transcriptomics analysis will identify others, perhaps with distinct roles in the ensemble encoding of metabolic state.[6] Defining which PVH populations receive increased input from AgRP neurons in HS^{PN} mice and identifying how enhanced innervation impacts downstream neuronal activity will help define the functional consequence of the developmental perturbation identified here. Together, the results from the TRAP2 experiments support a model in which ensembles of PVH neurons are co-activated by thirst signals conveyed by MEPO neurons and by hunger signals to coordinate drinking and feeding behavior.

Using postnatal treatment of HS to model dehydration in neonatal mice, we demonstrate functional connectivity during early postnatal development where the MEPO and PVH display Fos labeling in response to dehydration signals as early as P1, consistent with earlier studies in the rat that demonstrated robust Fos induction in the MEPO in response to HS at P2.[34] The ontogeny of functional connectivity between the MEPO and PVH is reflected in the progressive increases in Fos labeling in response to HS, where the maximum Fos induction we observe in the MEPO and PVH is at the end of the first and second week of life, respectively. This finding is consistent with the structural connectivity between the MEPO and PVH at P8 visualized with DiI labeling. Although the presence of direct projections from the MEPO to the PVH that precede inputs from the ARH suggests that dehydration signals may cause induction of Fos in postnatal mice, it remains possible that inputs from other regions, such as those derived from neurons in the subfornical organ, may share a similar ontogeny and contribute to observed Fos labeling in the PVH. Similarly, AgRP neurons do not appear to drive milk consumption until after the second week of life, coinciding with the exploration of solid food and the maturation

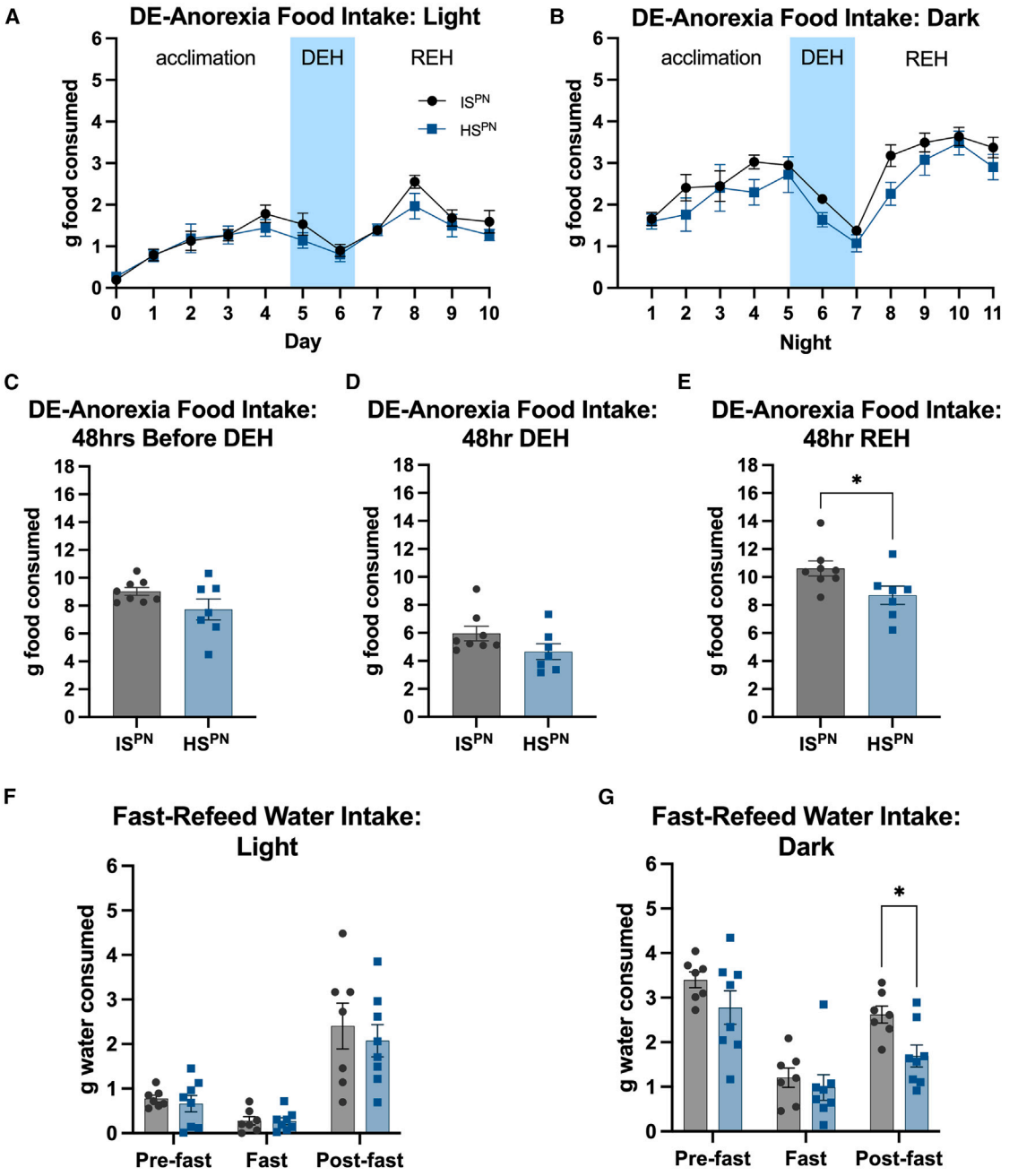

Figure 6. Hyperstimulation of drinking circuits during postnatal development leads to a sustained dehydration-anorexic response and a decrease in water intake after a fast-refeed in adult mice

(A) Quantification of daily food intake during the inactive light cycle of IS^{PN} mice ($n = 8$) and HS^{PN} mice ($n = 7$) for the acclimation period, dehydration period (DEH), and rehydration period (REH). two-way ANOVA: no significant effect of treatment over time. Data are presented as group mean values ±SEM.

(B) Quantification of nightly food intake during the active dark cycle of IS^{PN} ($n = 8$) and HS^{PN} ($n = 7$) for the acclimation period, dehydration period (DEH), and rehydration period (REH). two-way ANOVA: no significant effects of treatment over time. Data are presented as group mean values ±SEM.

(C) Quantification of food intake 48h before the dehydration period (acclimation). IS^{PN} ($n = 8$) and HS^{PN} ($n = 7$).

(D) Quantification of average food intake for the 48h dehydration period (DEH). IS^{PN} ($n = 8$) and HS^{PN} ($n = 7$).

(E) Quantification of food intake for the first 48h following rehydration (REH). IS^{PN} ($n = 8$) and HS^{PN} ($n = 7$).

(F) Quantification of water intake during the inactive light cycle before a fast, during the fast, and after refeeding. (IS^{PN} ($n = 7$) and HS^{PN} ($n = 8$).

(G) Quantification of water intake during the active dark cycle before a fast, during the fast, and after refeeding. (IS^{PN} ($n = 7$) and HS^{PN} ($n = 8$). Data for (C–G) are represented as mean ± SEM and data points are individual animals; n represents the number of animals; Unpaired t-test: $*p < 0.05$, $**p < 0.01$, $***p < 0.001$. See also Figure S5.

of projections from AgRP neurons to their targets, including the PVH.[19,61,64] Thus, the ontogeny of projections from the MEPO to the PVH corresponds to the ability of osmotic signals to activate PVH neurons and precedes the functional maturation of AgRP inputs from the ARH.

Developing hypothalamic neural circuits are vulnerable to environmental perturbations during postnatal critical periods.[39,40,43] For example, leptin-deficiency, suppressed AgRP activity, and maternal high fat diet during the postnatal critical period for development of AgRP neurons all result in reduced innervation of downstream neuronal targets.[19,47,48,54] In contrast, daily exposure to HS leads to an increase in AgRP innervation of the PVH and MEPO, suggesting that hyperstimulation of MEPO neurons promotes innervation of common targets by neurons involved in feeding and satiety. Whether the hyperinnervation of PVH neurons by AgRP afferents is due to a transsynaptic activation of PVH neurons or is due to activation of local guidance cues that promote innervation by AgRP neurons remains to be determined. The greater sensitivity of MEPO neurons to HS stimulation during early postnatal life is consistent with the possibility that observed changes in structural connectivity could be due to activity-dependent development mechanisms, similar to those observed previously for AgRP inputs to the PVH and associated leptin-dependent development of projections from the PVH oxytocin neurons to the brainstem.[56] Although it remains plausible that HS treatment increases the number of AgRP neurons in the ARH, we would not expect postnatal perturbations in nutrition or activity to alter numbers of AgRP neurons, because AgRP neurons are born during mid-gestation and mature primarily before birth.[41,51,73–75] Furthermore, postnatal hyperstimulation of MEPO neurons caused a decrease in β-endorphin fiber densities in the MEPO, but did not affect innervation of the PVH, suggesting that circuitry defects resulting from neonatal HS treatment extend beyond AgRP and display cell type specificity. Taken together, these findings suggest a model in which projections from AgRP neurons to the PVH develop during postnatal life under the influence of both cell autonomous activity, as well as that of activation of convergent inputs to PVH neurons derived from the MEPO. For example, stimulation of glutamatergic afferents to the PVH by MEPO neurons during development may lead to enhanced activity of PVH neurons that promotes convergent innervation by GABAergic AgRP neurons. Alternatively, stimulation of the MEPO may promote development of a descending glutamatergic input to the ARH, where hyperstimulation of AgRP neurons during development may lead to increased convergent innervation of PVH neurons. Although postnatal dehydration appears to be a novel model of developmental programming, additional work is required to define molecular mechanisms mediating the effects of postnatal dehydration on development of AgRP innervation patterns. AgRP and POMC neurons clearly represent programmable components of feeding circuits, but they are only one of many cell types involved in feeding. For example, evaluating possible changes in the strength of afferents to PVH neurons that express melanocortin receptors, or that are modulated by circulating hormones involved in metabolic regulation, will provide additional insight into changes imposed onto feeding circuitry by osmotic thirst during postnatal life.

In addition to observed changes in AgRP and POMC projections caused by postnatal exposure to osmotic dehydration, we also observed sustained changes to ingestive behavior displayed by HS^{PN} offspring in adulthood. During short-term HFD exposure, adult HS^{PN} mice showed enhanced water intake with no change in food intake or body weight. Moreover, deprivation of food with a fast-refeed challenge of adult HS^{PN} mice led to a sustained decrease in water consumption after food replacement. Furthermore, deprivation of water with a dehydration challenge of adult HS^{PN} mice led to a sustained anorexic response after water replacement with no changes to water intake, in sharp contrast to the normal reversal of dehydration-anorexia that follows water replacement in control mice. The sustained anorexic response in HS^{PN} mice may appear surprising in light of the enhanced innervation of the PVH by AgRP neurons. Such apparently discordant findings may be due to undefined changes to innervation of various populations of PVH neurons, or possible changes to the organization of local circuits in the PVH that result from HS^{PN} exposure. Nonetheless, the observed context-specific changes are consistent with prior studies of AgRP ablation leading to context-specific changes in food intake.[18,69] This is important because postnatal osmotic dehydration appears to disrupt the tight coupling of fluid homeostasis and food intake and appears to be context-specific.

Although the differences observed in the ingestive behavior challenges are quantitatively modest, the cumulative impact of circuitry changes caused by HS^{PN} exposure may lead to a significant change to the salience of specific cues impacting ingestive behaviors. Thus, these findings suggest that HS^{PN} may affect neuronal integration of signals controlling fluid homeostasis and hunger that are related to encoding responses to competing motivational states. One possible explanation is that changes to convergent circuits conveying thirst and hunger signals may alter the impact of negative valence signals that represent environmental cues associated with nutrient or water ingestion.[24,29,76] This interpretation is consistent with the observation that drinking was only perturbed in HS^{PN} mice during exposure to HFD and that food intake was only altered within the context of dehydration-anorexia. Alternatively, observed changes in ingestive behavior could be due to defects in anticipatory modulation, consistent with other findings that water intake changes with diet content.[11,13] Although tdTomato+/Fos+ labeling in the MEPO of our TRAP2 experiment may reflect the presence of neurons that respond to both dehydration and feeding-related stimuli, it is equally likely that the doubly-labeled neurons in the MEPO are due to the presence of reciprocal connections between the PVH and MEPO that coordinate drinking and feeding. Thus, metabolic information being conveyed to the MEPO may not be appropriately integrated in HS^{PN} mice due to structural changes in the neural circuits involved in feeding, resulting in changes to ingestive behavior during metabolic challenge. Collectively, our results support a model in which dehydration in early life not only leads to long-term structural changes in hypothalamic circuits, but also expression of context-specific functional deficits in coordinated ingestive behaviors.[77]

Drinking and feeding are highly coordinated behaviors, and we have identified a novel developmental interaction between neurons that sense osmotic challenges and AgRP circuits that

may contribute to environmentally-specified programming of context-specific ingestive behavior. The developmental activity demonstrated here for osmotic dehydration during postnatal life not only changes patterns of structural connectivity in the hypothalamus but exerts a lasting change to how fluid balance and food intake are coordinated during homeostatic stress. Thus, convergent neural inputs to the PVH from neurons in the MEPO and ARH may represent a developmental substrate that links early dehydration with sustained perturbation of fluid homeostasis and energy balance, adding osmotic disruptors to the growing list of agents that act during critical periods of development to program hypothalamic structural and functional connectivity. As water scarcity and dietary hypernatremia increase in vulnerable populations, this developmental exposure may have unforeseen consequences for how the brain coordinates multiple aspects of homeostasis.

Limitations of the study

The results of the TRAP2/Fos labeling studies in adult mice clearly identified neurons that respond to both thirst and feeding states, but the numbers and cellular identities of the neurons detected may be different with an analysis of Hunger-TRAP and Thirst-Fos. In the fast-refeed test, Fos-labeled neurons may also represent a composite population of cells that are activated in the fasted state and those activated by exposure to food. An alternative interpretation is that the Fos-labeled neurons represent cells that are involved in the transition from the fed to fasted state. Additional experimentation with *in vivo* imaging will be necessary to differentiate between these possibilities. Moreover, additional investigation is required to determine how postnatal dehydration affects neuronal signaling at the level of the PVH, as we observed a sustained decrease in food intake after dehydration-anorexia despite an increase in AgRP fiber densities in HS^{PN} mice. The PVH clearly serves as a node of integration for signals important for coordination of ingestive behavior, but it is part of a broader network of regions involved in homeostatic regulation that may be responsive to developmental programming by postnatal dehydration. Furthermore, the PVH controls secretion of several circulating hormones, such as corticosterone and vasopressin, which were not measured in this study and whose actions are likely overlaid onto the direct actions of AgRP innervation. A significant limitation of the present work is that the studies were conducted exclusively using male mice. This was done to avoid possible confounds caused by hormonal fluctuations that occur during the estrous cycle in female mice, but we appreciate that developmental differences in circuit formation exist between males and females that may also impact how dehydration affects development of feeding circuits.[78] Nevertheless, the studies reported here provide a foundation for future discovery into how multiple environmental signals can exert lasting effects on the functional anatomy of ingestive behavior.

RESOURCE AVAILABILITY

Lead contact

Further information and reasonable requests from qualified investigators for resources and reagents should be directed to and will be fulfilled by the lead contact, Richard B. Simerly: richard.simerly@vanderbilt.edu.

Materials availability

This study did not generate new unique reagents.

Data and code availability

- Image data have been deposited in Open Science Framework (https://osf.io/4rwge/). All data supporting the findings of this study will be shared by the lead contact upon request.
- This paper does not report original code.
- Any additional information required to reanalyze the data reported in this paper is available from the lead contact upon request.

ACKNOWLEDGMENTS

This research was supported by the National Institute of Diabetes and Digestive and Kidney Diseases (5R01DK106476 to RBS) and the Eunice Kennedy Shriver National Institute of Child Health and Human Development (5F31HD106890 to SRS).

Graphical abstract was made using BioRender: Created in BioRender. Sweet, S. (2025) https://BioRender.com/a29u060.

AUTHOR CONTRIBUTIONS

Conceptualization, S.R.S. and R.B.S.; methodology, S.R.S., R.B.S., and J.E.B.; investigation, S.R.S. and J.E.B.; formal analysis, S.R.S., J.B.Z., and G.L.Y.; resources, R.B.S.; writing – original draft, S.R.S. and R.B.S.; writing – review and editing, S.R.S., R.B.S., J.E.B., and J.B.Z.; visualization, S.R.S.; supervision, R.B.S.; funding acquisition, R.B.S.

DECLARATION OF INTERESTS

The authors declare no competing interests.

STAR★METHODS

Detailed methods are provided in the online version of this paper and include the following:

- KEY RESOURCES TABLE
- EXPERIMENTAL MODEL AND SUBJECT DETAILS
  - Animals
- METHOD DETAILS
  - Tissue preparation
  - Immunohistochemistry
  - DiI tracing studies
  - cFos experiments
  - Postnatal hypertonic saline treatments
  - TRAP induction
  - Food and water intake analysis
- QUANTIFICATION AND STATISTICAL ANALYSIS
  - Image acquisition and analysis
  - Statistical analysis and graphical display of data

SUPPLEMENTAL INFORMATION

Supplemental information can be found online at https://doi.org/10.1016/j.isci.2025.112284.

Received: October 24, 2024
Revised: January 24, 2025
Accepted: March 20, 2025
Published: March 24, 2025

REFERENCES

1. Sawchenko, P.E., and Swanson, L.W. (1981). Central Noradrenergic Pathways for the Integration of Hypothalamic Neuroendocrine and Autonomic

Responses. Science *214*, 685–687. https://doi.org/10.1126/science.7292008.

2. Swanson, L.W., and Sawchenko, P.E. (1983). Hypothalamic Integration: Organization of the Paraventricular and Supraoptic Nuclei. Annu. Rev. Neurosci. *6*, 269–324. https://doi.org/10.1146/annurev.ne.06.030183.001413.
3. Swanson, L.W., and Sawchenko, P.E. (1980). Paraventricular Nucleus:A Site for the Integration of Neuroendocrine and Autonomic Mechanisms. Neuroendocrinology *31*, 410–417. https://doi.org/10.1159/000123111.
4. Sawchenko, P.E., and Swanson, L.W. (1983). The organization of forebrain afferents to the paraventricular and supraoptic nuclei of the rat. J. Comp. Neurol. *218*, 121–144. https://doi.org/10.1002/cne.902180202.
5. Sawchenko, P.E., and Swanson, L.W. (1982). The organization of noradrenergic pathways from the brainstem to the paraventricular and supraoptic nuclei in the rat. Brain Res. *257*, 275–325. https://doi.org/10.1016/0165-0173(82)90010-8.
6. Xu, S., Yang, H., Menon, V., Lemire, A.L., Wang, L., Henry, F.E., Turaga, S.C., and Sternson, S.M. (2020). Behavioral state coding by molecularly defined paraventricular hypothalamic cell type ensembles. Science (New York, N.Y.) *370*, eabb2494. https://doi.org/10.1126/science.abb2494.
7. Watts, A.G. (1999). Dehydration-Associated Anorexia Development and Rapid Reversal. Physiol. Behav. *65*, 871–878. https://doi.org/10.1016/s0031-9384(98)00244-3.
8. Watts, A.G., Sanchez-Watts, G., and Kelly, A.B. (1999). Distinct patterns of neuropeptide gene expression in the lateral hypothalamic area and arcuate nucleus are associated with dehydration- induced anorexia. J. Neurosci. *19*, 6111–6121. https://doi.org/10.1523/jneurosci.19-14-06111.1999.
9. Boyle, C.N., Lorenzen, S.M., Compton, D., and Watts, A.G. (2012). Dehydration-anorexia derives from a reduction in meal size, but not meal number. Physiol. Behav. *105*, 305–314. https://doi.org/10.1016/j.physbeh.2011.08.005.
10. Watts, A.G., and Boyle, C.N. (2010). The functional architecture of dehydration-anorexia. Physiol. Behav. *100*, 472–477. https://doi.org/10.1016/j.physbeh.2010.04.010.
11. Fitzsimons, T.J., and Le Magnen, J. (1969). Eating as a regulatory control of drinking in the rat. J. Comp. Physiol. Psychol. *67*, 273–283. https://doi.org/10.1037/h0026772.
12. Krause, E.G., de Kloet, A.D., and Sakai, R.R. (2010). Post-ingestive signals and satiation of water and sodium intake of male rats. Physiol. Behav. *99*, 657–662. https://doi.org/10.1016/j.physbeh.2010.01.030.
13. Zimmerman, C.A., Lin, Y.C., Leib, D.E., Guo, L., Huey, E.L., Daly, G.E., Chen, Y., and Knight, Z.A. (2016). Thirst neurons anticipate the homeostatic consequences of eating and drinking. Nature *537*, 680–684. https://doi.org/10.1038/nature18950.
14. Thompson, R.H., and Swanson, L.W. (2003). Structural characterization of a hypothalamic visceromotor pattern generator network. Brain Res. Rev. *41*, 153–202. https://doi.org/10.1016/s0165-0173(02)00232-1.
15. Gong, R., Xu, S., Hermundstad, A., Yu, Y., and Sternson, S.M. (2020). Hindbrain Double-Negative Feedback Mediates Palatability-Guided Food and Water Consumption. Cell *182*, 1589–1605.e22. https://doi.org/10.1016/j.cell.2020.07.031.
16. Volcko, K.L., Brakey, D.J., McNamara, T.E., Meyer, M.J., McKay, N.J., Santollo, J., and Daniels, D. (2022). Control of water intake by a pathway from the nucleus of the solitary tract to the paraventricular hypothalamic nucleus. Appetite *172*, 105943. https://doi.org/10.1016/j.appet.2022.105943.
17. Gutman, M.B., Jones, D.L., and Ciriello, J. (1988). Effect of paraventricular nucleus lesions on drinking and pressor responses to ANG II. Am. J. Physiol. *255*, R882–R887. https://doi.org/10.1152/ajpregu.1988.255.6.r882.
18. Luquet, S., Perez, F.A., Hnasko, T.S., and Palmiter, R.D. (2005). NPY/AgRP Neurons Are Essential for Feeding in Adult Mice but Can Be Ablated in Neonates. Science *310*, 683–685. https://doi.org/10.1126/science.1115524.
19. Bouret, S.G., Draper, S.J., and Simerly, R.B. (2004). Formation of Projection Pathways from the Arcuate Nucleus of the Hypothalamus to Hypothalamic Regions Implicated in the Neural Control of Feeding Behavior in Mice. J. Neurosci. *24*, 2797–2805. https://doi.org/10.1523/jneurosci.5369-03.2004.
20. Aponte, Y., Atasoy, D., and Sternson, S.M. (2011). AGRP neurons are sufficient to orchestrate feeding behavior rapidly and without training. Nat. Neurosci. *14*, 351–355. https://doi.org/10.1038/nn.2739.
21. Krashes, M.J., Koda, S., Ye, C., Rogan, S.C., Adams, A.C., Cusher, D.S., Maratos-Flier, E., Roth, B.L., and Lowell, B.B. (2011). Rapid, reversible activation of AgRP neurons drives feeding behavior in mice. J. Clin. Investig. *121*, 1424–1428. https://doi.org/10.1172/jci46229.
22. Atasoy, D., Betley, J.N., Su, H.H., and Sternson, S.M. (2012). Deconstruction of a neural circuit for hunger. Nature *488*, 172–177. https://doi.org/10.1038/nature11270.
23. Wu, Q., Clark, M.S., and Palmiter, R.D. (2012). Deciphering a neuronal circuit that mediates appetite. Nature *483*, 594–597. https://doi.org/10.1038/nature10899.
24. Betley, J.N., Xu, S., Cao, Z.F.H., Gong, R., Magnus, C.J., Yu, Y., and Sternson, S.M. (2015). Neurons for hunger and thirst transmit a negative-valence teaching signal. Nature *521*, 180–185. https://doi.org/10.1038/nature14416.
25. Johnson, A.K., Zardetto-Smith, A.M., and Edwards, G.L. (1992). Chapter 50: Integrative mechanisms and the maintenance of cardiovascular and body fluid homeostasis: the central processing of sensory input derived from the circumventricular organs of the lamina terminalis. Prog. Brain Res. *91*, 381–393. https://doi.org/10.1016/s0079-6123(08)62357-2.
26. McKinley, M.J., Yao, S.T., Uschakov, A., McAllen, R.M., Rundgren, M., and Martelli, D. (2015). The median preoptic nucleus: front and centre for the regulation of body fluid, sodium, temperature, sleep and cardiovascular homeostasis. Acta Physiol. *214*, 8–32. https://doi.org/10.1111/apha.12487.
27. Oka, Y., Ye, M., and Zuker, C.S. (2015). Thirst driving and suppressing signals encoded by distinct neural populations in the brain. Nature *520*, 349–352. https://doi.org/10.1038/nature14108.
28. Abbott, S.B.G., Machado, N.L.S., Geerling, J.C., and Saper, C.B. (2016). Reciprocal control of drinking behavior by median preoptic neurons in mice. J. Neurosci. *36*, 8228–8237. https://doi.org/10.1523/jneurosci.1244-16.2016.
29. Leib, D.E., Zimmerman, C.A., Poormoghaddam, A., Huey, E.L., Ahn, J.S., Lin, Y.C., Tan, C.L., Chen, Y., and Knight, Z.A. (2017). The Forebrain Thirst Circuit Drives Drinking through Negative Reinforcement. Neuron *96*, 1272–1281.e4. https://doi.org/10.1016/j.neuron.2017.11.041.
30. Zimmerman, C.A., Leib, D.E., and Knight, Z.A. (2017). Neural circuits underlying thirst and fluid homeostasis. Nat. Rev. Neurosci. *18*, 459–469. https://doi.org/10.1038/nrn.2017.71.
31. Augustine, V., Gokce, S.K., Lee, S., Wang, B., Davidson, T.J., Reimann, F., Gribble, F., Deisseroth, K., Lois, C., and Oka, Y. (2018). Hierarchical neural architecture underlying thirst regulation. Nature *555*, 204–209. https://doi.org/10.1038/nature25488.
32. Zimmerman, C.A., Huey, E.L., Ahn, J.S., Beutler, L.R., Tan, C.L., Kosar, S., Bai, L., Chen, Y., Corpuz, T.V., Madisen, L., et al. (2019). A gut-to-brain signal of fluid osmolarity controls thirst satiation. Nature *568*, 98–102. https://doi.org/10.1038/s41586-019-1066-x.
33. Ding, J.M., Carver, W.C., Terracio, L., and Buggy, J. (1994). Proto-oncogene c-fos and the regulation of vasopressin gene expression during dehydration. Brain Res. Mol. Brain Res. *21*, 247–255. https://doi.org/10.1016/0169-328x(94)90255-0.
34. Rinaman, L., Stricker, E.M., Hoffman, G.E., and Verbalis, J.G. (1997). Central c-Fos expression in neonatal and adult rats after subcutaneous

injection of hypertonic saline. Neuroscience *79*, 1165–1175. https://doi.org/10.1016/s0306-4522(97)00022-5.

35. Cabral, A., Fernandez, G., Tolosa, M.J., Rey Moggia, Á., Calfa, G., De Francesco, P.N., and Perello, M. (2020). Fasting induces remodeling of the orexigenic projections from the arcuate nucleus to the hypothalamic paraventricular nucleus, in a growth hormone secretagogue receptor–dependent manner. Mol. Metab. *32*, 69–84. https://doi.org/10.1016/j.molmet.2019.11.014.
36. Salter-Venzon, D., and Watts, A.G. (2008). The role of hypothalamic ingestive behavior controllers in generating dehydration anorexia: A Fos mapping study. Am. J. Physiol. Regul. Integr. Comp. Physiol. *295*, 1009–1019. https://doi.org/10.1152/ajpregu.90425.2008.
37. Sutton Hickey, A.K., Duane, S.C., Mickelsen, L.E., Karolczak, E.O., Shamma, A.M., Skillings, A., Li, C., and Krashes, M.J. (2023). AgRP neurons coordinate the mitigation of activity-based anorexia. Mol. Psychiatry *28*, 1622–1635. https://doi.org/10.1038/s41380-022-01932-w.
38. de Araujo Salgado, I., Li, C., Burnett, C.J., Rodriguez Gonzalez, S., Becker, J.J., Horvath, A., Earnest, T., Kravitz, A.V., and Krashes, M.J. (2023). Toggling between food-seeking and self-preservation behaviors via hypothalamic response networks. Neuron *111*, 2899–2917.e6. https://doi.org/10.1016/j.neuron.2023.06.006.
39. Levin, B.E. (2000). The obesity epidemic: metabolic imprinting on genetically susceptible neural circuits. Obes. Res. *8*, 342–347. https://doi.org/10.1038/oby.2000.41.
40. Elson, A.E., and Simerly, R.B. (2015). Developmental specification of metabolic circuitry. Front. Neuroendocrinol. *39*, 38–51. https://doi.org/10.1016/j.yfrne.2015.09.003.
41. Zeltser, L.M., Seeley, R.J., and Tschöp, M.H. (2012). Synaptic plasticity in neuronal circuits regulating energy balance. Nat. Neurosci. *15*, 1336–1342. https://doi.org/10.1038/nn.3219.
42. Zeltser, L.M. (2018). Feeding circuit development and early-life influences on future feeding behaviour. Nat. Rev. Neurosci. *19*, 302–316. https://doi.org/10.1038/nrn.2018.23.
43. Bouret, S.G., Draper, S.J., and Simerly, R.B. (2004). Trophic Action of Leptin on Hypothalamic Neurons That Regulate Feeding. Science *304*, 108–110. https://doi.org/10.1126/science.1095004.
44. Bouret, S.G., and Simerly, R.B. (2007). Development of Leptin-Sensitive Circuits. J. Neuroendocrinol. *19*, 575–582. https://doi.org/10.1111/j.1365-2826.2007.01563.x.
45. Remmers, F., and Delemarre-van de Waal, H.A. (2011). Developmental programming of energy balance and its hypothalamic regulation. Endocr. Rev. *32*, 272–311. https://doi.org/10.1210/er.2009-0028.
46. Remmers, F., Fodor, M., and Delemarre-van de Waal, H.A. (2008). Neonatal food restriction permanently alters rat body dimensions and energy intake. Physiol. Behav. *95*, 208–215. https://doi.org/10.1016/j.physbeh.2008.05.021.
47. Kamitakahara, A., Bouyer, K., Wang, C.H., and Simerly, R. (2018). A critical period for the trophic actions of leptin on AgRP neurons in the arcuate nucleus of the hypothalamus. J. Comp. Neurol. *526*, 133–145. https://doi.org/10.1002/cne.24327.
48. Bouyer, K., and Simerly, R.B. (2013). Neonatal leptin exposure specifies innervation of presympathetic hypothalamic neurons and improves the metabolic status of leptin-deficient mice. J. Neurosci. *33*, 840–851. https://doi.org/10.1523/jneurosci.3215-12.2013.
49. Masuyama, H., and Hiramatsu, Y. (2014). Additive effects of maternal high fat diet during lactation on mouse offspring. PLoS One *9*, e92805. https://doi.org/10.1371/journal.pone.0092805.
50. Delahaye, F., Breton, C., Risold, P.Y., Enache, M., Dutriez-Casteloot, I., Laborie, C., Lesage, J., and Vieau, D. (2008). Maternal Perinatal Undernutrition Drastically Reduces Postnatal Leptin Surge and Affects the Development of Arcuate Nucleus Proopiomelanocortin Neurons in Neonatal Male Rat Pups. Endocrinology *149*, 470–475. https://doi.org/10.1210/en.2007-1263.
51. Bouret, S.G. (2022). Developmental programming of hypothalamic melanocortin circuits. Exp. Mol. Med. *54*, 403–413. https://doi.org/10.1038/s12276-021-00625-8.
52. Stevens, A., Begum, G., and White, A. (2011). Epigenetic changes in the hypothalamic pro-opiomelanocortin gene: A mechanism linking maternal undernutrition to obesity in the offspring? Eur. J. Pharmacol. *660*, 194–201. https://doi.org/10.1016/j.ejphar.2010.10.111.
53. Gali Ramamoorthy, T., Begum, G., Harno, E., and White, A. (2015). Developmental programming of hypothalamic neuronal circuits: impact on energy balance control. Front. Neurosci. *9*, 126. https://doi.org/10.3389/fnins.2015.00126.
54. Vogt, M.C., Paeger, L., Hess, S., Steculorum, S.M., Awazawa, M., Hampel, B., Neupert, S., Nicholls, H.T., Mauer, J., Hausen, A.C., et al. (2014). Neonatal insulin action impairs hypothalamic neurocircuit formation in response to maternal high-fat feeding. Cell *156*, 495–509. https://doi.org/10.1016/j.cell.2014.01.008.
55. Desai, M., Ferrini, M.G., Han, G., Narwani, K., and Ross, M.G. (2020). Maternal High Fat Diet Programs Male Mice Offspring Hyperphagia and Obesity: Mechanism of Increased Appetite Neurons via Altered Neurogenic Factors and Nutrient Sensor AMPK. Nutrients *12*, 3326. https://doi.org/10.3390/nu12113326. https://www.mdpi.com/2072-6643/12/11/3326.
56. Biddinger, J.E., Elson, A.E.T., Fathi, P.A., Sweet, S.R., Nishimori, K., Ayala, J.E., and Simerly, R.B. (2024). AgRP Neurons Mediate Activity Dependent Development of Oxytocin Connectivity and Autonomic Regulation. Proc. Natl. Acad. Sci. USA *121*, e2403810121. https://doi.org/10.1073/pnas.2403810121.
57. Simerly, R.B. (2008). Hypothalamic substrates of metabolic imprinting. Physiol. Behav. *94*, 79–89. https://doi.org/10.1016/j.physbeh.2007.11.023.
58. Fernandez-Twinn, D.S., and Ozanne, S.E. (2010). Early life nutrition and metabolic programming. Ann. N. Y. Acad. Sci. *1212*, 78–96. https://doi.org/10.1111/j.1749-6632.2010.05798.x.
59. Dearden, L., and Ozanne, S.E. (2015). Early life origins of metabolic disease: Developmental programming of hypothalamic pathways controlling energy homeostasis. Front. Neuroendocrinol. *39*, 3–16. https://doi.org/10.1016/j.yfrne.2015.08.001.
60. Dehorter, N., and Del Pino, I. (2020). Shifting Developmental Trajectories During Critical Periods of Brain Formation. Front. Cell. Neurosci. *14*, 283. https://doi.org/10.3389/fncel.2020.00283.
61. Bornstein, B.H., Terry, L.M., Browde, J.A., Jr., Assimon, S.A., and Hall, W.G. (1987). Maternal and nutritional contributions to infant rats' activational responses to ingestion. Dev. Psychobiol. *20*, 147–163. https://doi.org/10.1002/dev.420200205.
62. Phifer, C.B., Ladd, M.D., and Hall, W.G. (1991). Effects of hydrational state on ingestion in infant rats: Is dehydration the only ingestive stimulus? Physiol. Behav. *49*, 695–699. https://doi.org/10.1016/0031-9384(91)90304-7.
63. Swithers, S.E. (2003). Do metabolic signals stimulate intake in rat pups? Physiol. Behav. *79*, 71–78. https://doi.org/10.1016/s0031-9384(03)00106-9.
64. Zimmer, M.R., Fonseca, A.H.O., Iyilikci, O., Pra, R.D., and Dietrich, M.O. (2019). Functional Ontogeny of Hypothalamic Agrp Neurons in Neonatal Mouse Behaviors. Cell *178*, 44–59.e7. https://doi.org/10.1016/j.cell.2019.04.026.
65. Londei, T., Calci, M., and Leone, V.G. (1988). First experiences with solid food by mouse pups: Effects of age and the presence of the mother. Bollettino di zoologia *55*, 155–159. https://doi.org/10.1080/11250008809386612.
66. Allen, W.E., DeNardo, L.A., Chen, M.Z., Liu, C.D., Loh, K.M., Fenno, L.E., Ramakrishnan, C., Deisseroth, K., and Luo, L. (2017). Thirst-associated preoptic neurons encode an aversive motivational drive. Science *357*, 1149–1155. https://doi.org/10.1126/science.aan6747.

67. Szczepanska-Sadowska, E., Cudnoch-Jedrzejewska, A., and Wsol, A. (2020). The role of oxytocin and vasopressin in the pathophysiology of heart failure in pregnancy and in fetal and neonatal life. Am. J. Physiol. Heart Circ. Physiol. *318*, H639–H651. https://doi.org/10.1152/ajpheart.00484.2019.

68. Leibowitz, S.F., Hammer, N.J., and Chang, K. (1981). Hypothalamic paraventricular nucleus lesions produce overeating and obesity in the rat. Physiol. Behav. *27*, 1031–1040. https://doi.org/10.1016/0031-9384(81)90366-8.

69. Cai, J., Chen, J., Ortiz-Guzman, J., Huang, J., Arenkiel, B.R., Wang, Y., Zhang, Y., Shi, Y., Tong, Q., and Zhan, C. (2023). AgRP neurons are not indispensable for body weight maintenance in adult mice. Cell Rep. *42*, 112789. https://doi.org/10.1016/j.celrep.2023.112789.

70. Savić, B., Murphy, D., and Japundžić-Žigon, N. (2022). The Paraventricular Nucleus of the Hypothalamus in Control of Blood Pressure and Blood Pressure Variability. Front. Physiol. *13*, 858941. https://doi.org/10.3389/fphys.2022.858941.

71. Madrigal, M.P., and Jurado, S. (2021). Specification of oxytocinergic and vasopressinergic circuits in the developing mouse brain. Commun. Biol. *4*, 586. https://doi.org/10.1038/s42003-021-02110-4.

72. Bourque, C.W. (2008). Central mechanisms of osmosensation and systemic osmoregulation. Nat. Rev. Neurosci. *9*, 519–531. https://doi.org/10.1038/nrn2400.

73. Khachaturian, H., Alessi, N.E., Lewis, M.E., Munfakh, N., Fitzsimmons, M.D., and Watson, S.J. (1985). Development of hypothalamic opioid neurons: A combined immunocytochemical and [3H]thymidine autoradiographic study. Neuropeptides *5*, 477–480. https://doi.org/10.1016/0143-4179(85)90058-7.

74. Padilla, S.L., Carmody, J.S., and Zeltser, L.M. (2010). Pomc-expressing progenitors give rise to antagonistic neuronal populations in hypothalamic feeding circuits. Nat. Med. *16*, 403–405. https://doi.org/10.1038/nm.2126.

75. Schwartz, G.J., and Zeltser, L.M. (2013). Functional Organization of Neuronal and Humoral Signals Regulating Feeding Behavior. Annu. Rev. Nutr. *33*, 1–21. https://doi.org/10.1146/annurev-nutr-071812-161125.

76. Burnett, C.J., Funderburk, S.C., Navarrete, J., Sabol, A., Liang-Guallpa, J., Desrochers, T.M., and Krashes, M.J. (2019). Need-based prioritization of behavior. Elife *8*, e44527. https://doi.org/10.7554/elife.44527.

77. Volcko, K.L., Brakey, D.J., Przybysz, J.T., and Daniels, D. (2020). Exclusively drinking sucrose or saline early in life alters adult drinking behavior by laboratory rats. Appetite *149*, 104616. https://doi.org/10.1016/j.appet.2020.104616.

78. Simerly, R.B. (2002). WIRED FOR REPRODUCTION: Organization and Development of Sexually Dimorphic Circuits in the Mammalian Forebrain. Annu. Rev. Neurosci. *25*, 507–536. https://doi.org/10.1146/annurev.neuro.25.112701.142745.

79. Guenthner, C.J., Miyamichi, K., Yang, H., Heller, H., and Luo, L. (2013). Permanent genetic access to transiently active neurons via TRAP: Targeted recombination in active populations [Neuron 78 (2013) 773-784]. Neuron *79*, 1257. https://doi.org/10.1016/j.neuron.2013.08.031.

80. Madisen, L., Zwingman, T.A., Sunkin, S.M., Oh, S.W., Zariwala, H.A., Gu, H., Ng, L.L., Palmiter, R.D., Hawrylycz, M.J., Jones, A.R., et al. (2010). A robust and high-throughput Cre reporting and characterization system for the whole mouse brain. Nat. Neurosci. *13*, 133–140. https://doi.org/10.1038/nn.2467.

81. Biddinger, J., Lazarenko, R., Scott, M., and Simerly, R. (2020). Leptin Suppresses Development of GLP-1 Inputs to the Paraventricular Nucleus of the Hypothalamus. Elife, 1–24. https://doi.org/10.1101/2020.06.30.180513.

STAR★METHODS

KEY RESOURCES TABLE

REAGENT or RESOURCE	SOURCE	IDENTIFIER
Antibodies		
Goat anti-AgRP	R&D Systems	Cat# AF704; RRID:AB_355537
Rabbit anti-β-endorphin	Phoenix Pharmaceuticals	Cat# H-022-33; RRID:AB_2314007
Rabbit anti-cFos	Cell Signaling	Cat# 2250; RRID:AB_2247211
Rabbit anti-nNOS	Immunostar	Cat#24431 RRID:AB_572255
Rabbit anti-oxytocin	Phoenix Pharmaceuticals	Cat# H-051-01 RRID:AB_2876858
Rabbit anti-vasopressin	Abcam	Cat#ab213708 RRID:AB_3099753
Alexa Fluor 488 anti-goat secondary antibody	Invitrogen	Cat# A32814; RRID:AB_2762838
Alexa Fluor 488 anti-rabbit secondary antibody	Invitrogen	Cat# A32790; RRID:AB_2762833
Alexa Fluor 568 anti-rabbit secondary antibody	Invitrogen	Cat# A10042; RRID:AB_2534017
Deposited data		
Images from figures	Open Science Framework	https://osk.io/4rwge/
Chemicals, peptides, and recombinant proteins		
4-hydroxy-tamoxifen	Sigma Aldrich	Cat# H6278; CAS 68392-35-8
DiI Stain (1,1′-Dioctadecyl-3,3,3′,3′-Tetramethylindocarbocyanine Perchlorate ('DiI"; $DiIC_{18}(3)$))	Invitrogen	Cat# D3911
Hoechst 33528	Molecular Probes	Cat# H3569; CAS 23491-45-4
NeuroTrace 640/660 Deep-Red Fluorescent Nissl Stain	Invitrogen	Cat# N21483
Experimental models: Organisms/strains		
Mouse: Wild-type C57BL/6J	Jackson Laboratories	Stock #000664 RRID:MGI:3028467
Mouse: Fos^{TRAP2} (B6.129(Cg)-$Fos^{tm1.1(cre/ERT2)Luo}$/J	Jackson Laboratories; Guenthner et al., Neuron 2013, [79]	Stock #021882 RRID:IMSR_JAX:021882
Mouse: Ai14(RCL-tdT)-D reporter mice B6.Cg-*Gt(ROSA)26Sor*$^{tm14(CAG-tdTomato/Hze}$/J	Jackson Laboratories; Madisen et al., Nature Neuroscience 2010, [80]	Stock #007914 RRID:IMSR_JAX:007914
Software and algorithms		
ZEN	Zeiss	https://www.zeiss.com/microscopy/us/products/software/zeiss-zen.html RRID:SCR_013672
Imaris v9.9.1	Oxford Instruments	http://www.bitplane.com/imaris/imaris RRID:SCR_007370
GraphPad Prism v10	GraphPad Software	https://www.graphpad.com/ RRID:SCR_002798
Illustrator v28.5	Adobe	RRID:SCR_010279
Other		
BioRender	BioRender	http://biorender.com RRID:SCR_018361

EXPERIMENTAL MODEL AND SUBJECT DETAILS

Animals

All animal care and experimental procedures were performed in accordance with the National Institutes of Health Guide for the Care and Use of Laboratory Animals (Garber et al., 2011) and approved by the Institutional Care and Use Committee at Vanderbilt

University (Ethical approval reference number M2300065-00-S2400544). Mice were housed at 22°C on a 12h light-dark cycle and provided *ad libitum* access to water and standard chow diet (PicoLab Rodent Diet 20, #5053), unless otherwise noted. Mice were weaned at P21 and maintained with mixed genotype littermates until males were used for experiments.

Wild-type (C57BL/6J; stock #000664) male mice at P1, P8, P16, and P30 were used for the acute dehydration and DiI experiments and at P48-60 for postnatal dehydration experiments. Male adult (8–12 weeks of age) Fos^{TRAP2} (B6.129(Cg)-$Fos^{tm1.1(cre/ERT2)Luo}$/J; stock #021882) mice expressing an inducible Cre-recombinase were crossed with Ai14(RCL-tdT)-D reporter mice (B6.Cg-*Gt(ROSA)26Sor*$^{tm14(CAG-tdTomato/Hze}$/J; stock #007914) to induce the tdTomato fluorescent protein in neurons activated by dehydration. Fos^{TRAP2} mice were heterozygous for both the $Fos^{2A-iCreER}$ and Ai14 alleles. All mice were obtained from the Jackson Laboratory.

METHOD DETAILS

Tissue preparation

Mice were perfused and processed for histochemical experiments as previously described b by Biddinger et al. and Bouyer & Simerly,[48,81] unless otherwise specified. Briefly, mice were first anesthetized with tribromoethanol (TBE), then perfused transcardially with 0.9% saline followed by ice-cold fixative (4% paraformaldehyde in 0.1M borate buffer, pH 9.5) for 20 min. Brains were carefully removed from the skull and postfixed in the same fixative for 4 h at 4°C.

For immunohistochemical studies, brains were cryoprotected overnight in 20% sucrose and a sliding microtome was used to collect 30μm thick coronal sections from brains derived from adult mice (P48-P60), or 50μm thick sections from brains collected at postnatal ages (P1-P30). The free-floating sections were stored in cryoprotectant solution at −20°C until further processing.

For DiI tracing studies, brains were stored in fixative at 4°C until DiI implantation. To prepare the brains for DiI implantation, the brains were mounted in a 3% agarose solution made in 0.02M KPBS. Brains were mounted onto a vibratome stage and sectioned from rostral to caudal so as to expose the median preoptic nucleus (MEPO). Single DiI crystals were implanted into the MEPO using an insect needle, and the brains were placed back into fixative and incubated for 5–6 weeks at 37°C. After incubation, brains were sectioned on a vibratome at 80μm.

Immunohistochemistry

To prepare the tissue for immunohistochemical processing, tissue sections were removed from cryoprotectant and rinsed in 0.02M KPBS. Sections were incubated overnight at 4°C in a 0.02M KPBS blocking buffer containing 2% normal donkey serum (Jackson ImmunoLabs) and 0.3% Triton X-100. Primary antibodies were diluted in blocking buffer, and used at the following concentrations: goat anti-AgRP (1:1000; R&D Systems), rabbit anti-β-endorphin (1:5000; Phoenix Pharmaceuticals), rabbit anti-cFos (1:1000; Cell Signaling), rabbit anti-nNOS (1:10,000; Immunostar), rabbit anti-oxytocin (1:1000; Phoenix Pharmaceuticals), and rabbit anti-vasopressin (1:500; Abcam). Tissue sections were incubated in blocking buffer containing combinations of primary antibodies for 48 h at 4°C. Sections were rinsed in 0.02M KPBS, and then incubated in the appropriate species-specific fluorophore-conjugated Alexa Fluor secondary antibodies for 1 h at RT. Tissue sections were rinsed again in 0.02M KPBS and counterstained with Hoechst Dye and/or NeuroTrace, and rinsed in 0.02M KPBS. Tissue sections were mounted directly onto charged Superfrost Plus slides (Fisher Scientific), and after drying overnight at 4°C were coverslipped with No.1.5 Gold Seal cover glass (Electron Microscopy Services) and ProLong Gold antifade mounting medium (Invitrogen).

DiI tracing studies

Free-floating tissue sections were collected by using a vibratome and counterstained at 1:10000 with Hoechst Dye in 0.02M KPBS. Tissue sections were rinsed in 0.02M KPBS and then mounted directly onto charged Superfrost Plus slides and coverslipped with glycerol buffer.

cFos experiments

cFOS immunostaining was used to assess location of activated neurons in response to dehydration and food deprivation. Briefly, age-matched groups of mice received subcutaneous (s.c.) injections of sterile hypertonic saline (2.0M NaCl) or isotonic saline (0.9% NaCl) on P1, P8, P16, or P28 for the postnatal studies; intraperitoneal (i.p.) injections of 250μL of 2.0M NaCl (P48-P80) for IS/HS^{PN} anatomical studies; and a 23h fast followed by a refeed was used for the Hunger-Fos paradigm. Mice were anesthetized with TBE 60 min later, perfused, and tissue processed for immunohistochemistry as described above.

Postnatal hypertonic saline treatments

Wild-type mouse litters were adjusted to 6–8 pups. Neonatal mice were weighed daily and remained in their home cage with their littermates and biological dam, with *ad libitum* access to standard rodent chow and water. To activate neuronal circuits involved in drinking via osmotic challenge, mice received daily subcutaneous (s.c.) injections of either hypertonic saline (2.0M NaCl, HS) or isotonic saline as a control (0.9% NaCl, IS) either postnatally (PN) from P5-P15 (HS^{PN} and IS^{PN}) or postweaning (PW) from P28-P38 (HS^{PW} and IS^{PW}). Injections were administered in the home cage, at least 1h prior to lights out. HS^{PN} and IS^{PN} mice were weaned onto the same chow diet at P21 and maintained on chow diet into adulthood. HS^{PW} and IS^{PW} were previously weaned at P21 and

maintained on chow diet into adulthood as well. Upon completion of physiological testing in adulthood, mice were perfused and processed for immunohistochemistry as described above.

TRAP induction

Adult *TRAP2;Ai14* mice were singly housed the week prior to utilization, and experiments were carried out in the homecage. All mice underwent a handling acclimation procedure daily, with an i.p. injection of 0.9% NaCl, for five days prior to the Thirst-TRAP experiment. 4-hydroxytamoxifen (4-OHT) was dissolved at 20 mg/mL in ethanol by shaking at 37°C for 15 min and the dissolved 4-OHT was then stored at −20°C until used. Before use, the dissolved 4-OHT was mixed with corn oil, shaken at 37°C, and ethanol evaporated for a final concentration of 10 mg/mL. For Thirst-TRAP studies, the final 10 mg/mL 4-OHT solution was injected i.p. at a dose of 50 mg/kg (Allen et. Al 2017) 30h after water bottles were removed from the cage. Water was returned 6h after 4-OHT injection. Mice were carefully observed for signs of distress or ill health during the water deprivation period. To identify neurons that display enhanced Fos labeling following a fast-refeed (Hunger-Fos), after 1 week of recovery from Thirst-TRAP, food was removed from the homecage. Mice were fasted for 23h before food was replaced to drive feeding. The fast-refeed captures the maximal number of neurons involved in the transition between the convergent states that drive feeding. 60 min after refeeding, mice were perfused and processed for immunohistochemical localization of Fos induction, as described above.

Food and water intake analysis

All mice used in Promethion Core System (Sable Systems International) studies, unless otherwise stated, were adults treated daily from P5-P15 with either hypertonic saline (HS^{PN}; 2.0M NaCl) or isotonic saline (IS^{PN}; 0.9% NaCl) as described above. As adults, mice were placed in individual cages the week prior to Sable testing, with *ad libitum* access to standard rodent chow and water. Mice were then singly housed in Promethion cages placed inside a temperature-controlled cabinet for the duration of the metabolic experiments described below and returned to their respective homecages following the conclusion of each experiment.

For the short-term high-fat diet challenge, mice were singly housed in Promethion cages and acclimated to the temperature-controlled cabinet for collection of baseline metabolic measurements for 5 days. A high-fat diet (40%, Research Diets) was then introduced for 7 days with continuous measurement of food and water intake.

For the long-term high-fat diet challenge, mice were singly housed in regular cages, not Promethion Core System cages, and provided *ad-libitum* access to high-fat diet (40%, Research Diets) for 20 weeks. Body weights were recorded for each animal once per week.

For the dehydration-anorexia challenge to study effects on ingestive behavior with water deprivation, mice were singly housed in Promethion cages and acclimated to the temperature-controlled cabinet for collection of baseline food and water intake for 4 days. The water bottle was then removed for 48h, and the mice were carefully observed for signs of distress or ill health every 8h during the water deprivation period. The water bottle was then re-introduced into the cage and continuous measurements of food and water intake were collected for 4 days.

For the fast-refeed challenge to study effects on ingestive behavior with food deprivation, mice were singly housed in Promethion cages and acclimated to the temperature-controlled cabinet After collection of baseline food and water intake, food was removed for 24h. Food was then re-introduced into the cage and continuous measurements of food and water intake were collected for a post-fast period of 24h.

QUANTIFICATION AND STATISTICAL ANALYSIS

Image acquisition and analysis

Brain tissue sections containing the MEPO, PVH, and ARH were identified and examined on a laser scanning confocal microscope (Zeiss LSM 800). Cytoarchitectonic features of these nuclei and subnuclei were visualized and identified with nuclear Hoechst Dye and/or cytoplasmic NeuroTrace to define matching regions of interest (ROIs) for quantitative analysis. Anatomically defined ROIs were used to quantify the density of labeled AgRP axons as well as cFOS in the MEPO, PVH, and ARH. In order to visualize and quantify AgRP axon densities in the PVH and MEPO of adult mice, sections were imaged at high magnification using an oil-immersion 40x objective, at a frequency of 0.08μm in the x and y planes and z-step of 0.427 with a digital zoom of 0.8x-1.0x. All other images were captured with a 20x objective and collected at a frequency of 1.18μm in the x and y planes, and a z-step of 1.38μm, with a digital zoom of 0.8x unless otherwise noted.

Imaris (Bitplane V9.0) visualization software was used to prepare 3D reconstructions of each multichannel set of images. To quantify the overall densities of labeled AgRP and β-endorphin fibers in the ROI of the MEPO and PVH, the spots function in Imaris was used. The spots function allows for elimination of intervaricose segments by segmenting the image so that the resulting objects are analyzed with both shape and size filters to create labeled profiles to measure the density of AgRP terminals and varicosities within the ROI. To quantify the number of Fos nuclei in the MEPO and PVH induced by HS injection or Thirst-TRAP, the number of Fos nuclei was counted in a maximum projection image of confocal images through each ROI of each region, guided by the spots function in Imaris software.

Statistical analysis and graphical display of data

Statistical analyses were performed using GraphPad Prism software (Version 9.5). Food and water intake data were analyzed using repeated-measures ANOVA tests to compare data between groups over multiple time points; unpaired t-tests were used to compare data for all other statistical tests. Data are presented as group mean values ±SEM, as well as individual data points, where n represents the number of animals in all studies and all dots on plots represent individual animals. Differences between groups were considered statistically significant at $p < 0.05$, and denoted by asterisks where $^{*}p < 0.05$, $^{**}p < 0.01$, $^{***}p < 0.001$. Details about statistical analyses details can be found in the figure legends. The Median Absolute Deviation (MAD) statistical method was used to detect outliers in datasets used for food and water intake analysis, with a 3.0 threshold (Leys et al. 2013). The median is a measure of central tendency that is insensitive to the presence of outliers compared to using the mean as a measure of central tendency. Graphs were constructed with GraphPad Prism (v10; GraphPad Software). Figure layouts were organized using Illustrator (v28.5; Adobe Systems). Photoshop was also used to adjust brightness and contrast on confocal images (v25.11; Adobe Systems).